Editors' Highlight

Electrochemical Detection of Single Microbeads Manipulated by Optical Tweezers in the Vicinity of Ultramicroelectrodes

Emmanuel Suraniti, Frédéric Kanoufi, Charlie Gosse, Xuan Zhao, Rumiana Dimova, Bernard Pouligny, and Neso Sojic

Anal. Chem., **Just Accepted Manuscript** • DOI: 10.1021/ac402200p • Publication Date (Web): 10 Sep 2013

Electrochemical Detection of Single Microbeads Manipulated by Optical Tweezers in the Vicinity of Ultramicroelectrodes

Emmanuel Suraniti,[1] *Frédéric Kanoufi,*[2] *Charlie Gosse,*[3] *Xuan Zhao,*[3] *Rumiana Dimova,*[4] *Bernard Pouligny,*[5] *Neso Sojic*[1, *]

1. Univ. Bordeaux, ENSCBP, ISM, UMR CNRS 5255, 33607 Pessac, France

2. ESPCI ParisTech, PECSA, UMR CNRS 7195, 75231 Paris Cedex 5, France

3. Laboratoire de Photonique et de Nanostructures, LPN-CNRS, 91460 Marcoussis, France.

4. Max Planck Institute of Colloids and Interfaces, Science Park Golm, 14424 Potsdam, Germany

5. Univ. Bordeaux, Centre de Recherche Paul Pascal, CNRS UPR 8641, 33607 Pessac, France

Corresponding Author: Prof. Neso SOJIC. Univ. Bordeaux, ENSCBP, ISM, UMR CNRS 5255, 33607 Pessac, France. Email: sojic@enscbp.fr

ABSTRACT

Latex micrometric beads are manipulated by optical tweezers in the vicinity of an ultramicroelectrode (UME). They are optically trapped in solution and approached to the electrode surface. After the electrochemical measurement, they are optically removed from the surface. The residence time of the particle on the electrode is thus controlled by the optical tweezers. The detection is based on diffusional hindrance by the insulating objects which alters the fluxes of the redox $Ru(NH_3)_6^{3+}$ species towards the UME and thus its mass-transfer limited current. We have optically deposited successively 1, 2 and 3 beads of 3-µm radius on the UME surface and we have recorded the variations of the current depending on their landing locations that were optically controlled. Finally we decreased the current by partially blocking the electroactive surface with a 6-bead assembly. The variation of the steady-state current and the approach curves allow for the indirect electrochemical localization of the bead in the vicinity of the UME, not only when the bead is in contact but also when it is levitated at distances lower than the UME radius. These experiments show that single particles or more complex structures may be manipulated *in situ* in a contactless mode near the UME surface. From comparison with simulations, the electrochemical detection affords an indirect localization of the object in the UME environment. The developed approach offers a potential application for interrogating the electrochemical activity of single cells and nanoparticles.

INTRODUCTION

Electrochemistry of nano- and microparticles is of high interest for detecting the presence, the size or the chemical signature of single objects. It is also a powerful approach to understand diffusion and reaction in the vicinity of individual objects or in confined volumes such as microbead agglomerates or nanoparticle opals.[1-12] Detection of single particle has thus been achieved using electrochemical techniques with both signal-on and signal-off approaches.[13-21] For example, Compton et al. have extensively studied the effect of inert particles blocking the surface of an electrode.[22] The authors positioned mechanically a bead of radius 125 µm on an electrode of radius 59 µm and studied its influence on cyclic voltammograms at different scan rates.[23,24] They were first able to extract the size of the particle from the voltammetric data. Thereafter, they even could monitor the motion of a moving particle across an electrode array.[24,25] Discrete adsorption events corresponding to the binding of individual inert micro- and nano-particles to the electrode have also been reported using amperometric detection.[16,20] The detection is here based on the blocking effects of diffusion of a redox probe induced by single beads approaching the electrode surface. Recently, Crooks and co-workers reported the fluorescence tracking of micrometric beads during their collisions with an ultramicroelectrode (UME).[21] Powerful methods for observing metallic nanoparticle collisions with the electrode surface have also been described based on the electrocatalytic amplification of the signal.[14,15,17-19] For instance, a Pt nanoparticle catalyzes proton reduction during its collision with a non-catalytic electrode surface and thus it leads to an enhancement of the current.[15] Similarly, electrogenerated chemiluminescence is enhanced when a Pt nanoparticle is in contact with an indium tin oxide (ITO) electrode and catalyzes the oxidation of the luminophore and of the co-reactant to finally generate the light emission.[14] However, the above cited reports exhibit an important limitation: the collision of the particles with the surface is a random process without precise control of the residence time or the rate of approaching the electrode. In this case, the frequency of the events is directly related to the concentration of the

nanoparticles in solution. Nevertheless, if the beads are positively or negatively charged, they may be attracted to the electrode surface by electromigration, depending on the applied potential.[16,20,21] For example, electrophoretic capture and detection of nanoparticles have been reported at nanopore electrodes.[26,27]

If electrochemical detection of single micro/nano-objects provides the screening of their activity and size, analysis at high throughput requires efficient and controlled ways to trap these objects in an electrode environment. Magnetic field trapping is popular in bioanalytical sciences and biophysics;[28] it is however restricted to paramagnetic beads presenting sufficient susceptibility. Optical tweezers are flexible tools that allow the trapping of micro- and nanoscopic objects non-invasively.[29-32] As a further advantage, it also affords the straightforward 3D displacement and therefore controlled positioning of the objects. Numerous applications ranging from fundamental physics to the medical sciences have been extensively reported. Various versions have been developed using single- and double-beam setups.[29,30] More sophisticated geometries may also generate multiple simultaneous traps and this technique progressively becomes a standard optical tool. The basic principles are based on the radiation pressure of the light and gradient forces. A simple and powerful configuration to form an optical trap is to focus tightly a laser beam with an objective lens of high numerical aperture.[31] Small objects with diameter from 0.1 μm to 20 μm, such as particles, living cells or subcellular components are easily trapped and manipulated in 3D. Optical manipulation is a particularly elegant tool since it works in a contactless mode.

In the present work, we used a single-beam optical tweezers and an optical levitation setup to manipulate latex microbeads in the vicinity of a transparent ITO UME (Figure 1). Liu et al. reported recently the electrochemical characterization of a bacterial cell trapped with optical tweezers.[33] They measured the direct electrical connection between the cell and the electrode. The focus of our work is to investigate the electrochemical effects of inert beads that are manipulated in the vicinity of an UME using optical tweezers and in this way to establish a calibration system for measurements on cells and

on nanoparticles. Latex microbeads were chosen as a model system because they are electrochemically inert, easy to trap optically and of same dimension as typical living cells. Optical tweezers were applied to position 1 to 6 microbeads near a static UME. Cyclic voltammetry was used to study the influence of the bead sizes, location, and packing on the steady-state amperometric UME response. The reported electrochemical configuration is related conceptually to the feedback mode of the Scanning Electrochemical Microscopy (SECM) where an UME is moved toward a substrate. The relative position of the substrate and its activity are obtained from its perturbation of the diffusional fluxes of a redox analyte to the UME surface. With the optical tweezers ensuring positioning control, the UME is static and inert objects are manipulated in its vicinity. Equivalently to SECM and as presented in Figure 1B, the insulating microbeads are expected to alter the diffusional fluxes of the electroactive species and thus the intensity of the electrochemical signal.[1,9,22] The diffusion hindrance afforded by a single bead or an assembly of beads is then analyzed electrochemically depending on their levitating or landing locations.

EXPERIMENTAL SECTION

Microfabrication of the transparent ITO UMEs.

The UME microfabrication (Figure S1) is a three main-step process which starts from 22 mm x 22 mm square borosilicate substrates, 175 μm thick, that have been coated by a ~ 100 nm ITO thin film of resistivity 20 ± 3 Ω/□ (PGO). First, the semiconductor surface is buried under 300 nm of silica relying on plasma enhanced chemical vapor deposition in a ND200 reactor (Nextral) using a 6:7:1 mixture of He, N_2O, and SiH_4 (total gas flow 140 sccm, pressure 640 mTorr, 13.56 MHz RF power 100 W, DC bias amplitude -55 V, and cathode temperature 280°C). Second, four corner-shaped gold marks are deposited using a standard lift-off protocol. The latter feature will facilitate the localization of the transparent and tiny electrode during bead micromanipulation under the optical microscope. Third, a

layer of AZ5214E (MicroChemicals) is patterned by photolithography to provide a hole 3, 6, or 12 μm in diameter. The ITO UME (see Figure 1 for the device general layout) is next obtained by removing the unprotected silicon oxide overlayer by reactive ion etching in a NE100 reactor (Nextral) using a 1:1 mixture of SF_6 and CHF_3 (total gas flow 16 sccm, pressure 10 mTorr, 13.56 MHz RF power 15 W, DC bias amplitude -150 V, and cathode temperature 18°C). It concomitantly allows one to define a large connecting pad for electrical interfacing with a potentiostat. Noticeably, thanks to alignment features located on both optical masks, the gold marks and the circular hole can be perfectly centered with respect to each other. Eventually, the glass slide is immersed in an acetone ultrasonic bath to get rid of the resist, flushed with isopropyl alcohol, and dried under a nitrogen flow. Before use, the wafer is dipped in chromic-sulfuric acid (VWR International) for 8 min, rinsed in water, rinsed in isopropyl alcohol, and finally dried under nitrogen flow.

Electrochemical cell

The transparent ITO UME itself constitutes the bottom of the electrochemical chamber. As it was designed to be transparent, it allows for both bead manipulation with a laser beam and observation of the sample from below by transmission optical microscopy. The body of the cell is composed of two pieces of PDMS stuck together following a plasma treatment prior to assembling with the electrode. The first layer, directly in contact with the silica of the electrode, is made of a thin film of PDMS in which a 1 mm diameter circular hole was punched. A 1cm wide and 5mm deep PDMS rectangular well is stuck above the first one. The cell in this configuration is “open” (Figure S2); this is the type used in optical tweezers experiments. In laser levitation experiments, a top glass is added making the cell closed. The well is wide enough to position a platinum wire as counter-electrode and an Ag/AgCl (3M KCl) reference electrode, which together with the ITO working UME form a classical 3-electrode set-up. Cyclic voltammograms were recorded with a μ-Autolab potentiostat (EcoChemie) in a solution containing $Ru(NH_3)_6Cl_3$ and Na_2SO_4 (Sigma-Aldrich).

Optical tweezers setups

Two optical manipulation setups were used in this work: the first one with a weakly focused beam and a reflexion interference contrast method (RICM) to levitate and to locate the bead, the second one with a tightly focused beam for the static beads positioned on the UME surface.

In the levitation experiments, a green laser beam (λ_G = 514 nm) propagates vertically through the cell, in upward direction (z), and is centred on the UME. The beam is only weakly focused (beam-waist ω_0 = 6 μm). This setup is derived from the early design of Ashkin *et al.* for optical levitation of dielectric particles.[34,35] The configuration acts as a 2-dimensional trap, and allows lifting up the particle, provided that enough laser power is applied. It does not provide real trapping in vertical direction, but it suffices to bring the particle up to any given altitude ($z > 0$). The distance z between the particle bottom and the UME is measured by means of an interference signal, following the principle of RICM.[36] The interference is built with an auxiliary probe laser beam (wavelength λ_R= 633 nm). The red beam is coaxial to the levitation beam and directed downwards. (See Figures S3-S4 and also Supporting Information for a detailed description). In levitation experiments, a bead was initially captured along the laser beam axis, then lifted up to a finite z, and left to sediment back to the UME surface (see Supporting Information for details).

The second optical setup which was used for the static experiments was installed on an inverted microscope (Zeiss Axiovert 200M). The trap was designed to be operated in the single beam mode as depicted on Figure 1A (i.e. the common optical tweezers geometry).[37] Briefly, the optical trap is fed by a continuous-wave YAG laser (λ= 1064 nm) through a high-numerical aperture (NA = 1.25) 63X immersion objective (Antiflex Plan Neofluar). The position of the beam inside the chamber can be adjusted horizontally (x, y) by means of a couple of computer controlled galvano-scanning mirrors acting on the beam upstream of the microscope. An alternative method consists in keeping the beam fixed and moving the sample with a motorized (x, y) stage. Along the optical axis, the distance between the beam focus and the cell bottom can be controlled as well, either through the microscope focus knob,

with a 50 nm resolution, or by means of an additional *z*-positioning stage attached to the (*x, y*) stage. Polystyrene beads (Polyscience) of different radii were injected in the transparent electrochemical cell containing the redox species. In the optical tweezers experiments, a bead was optically trapped close to the laser focus and then positioned on the surface of the UME. The laser was switched off prior to recording of the electrochemical signal.

Numerical simulation

Simulated electrode currents and electrogenerated redox probe concentration profiles were obtained by finite elements method with COMSOL 3.5 package (see details in Supporting Information). Computations were carried out in the 3D geometry. As sketched in Figure 1, the UMEs have a base radius r_e which is taken for the simulation procedure as unity (r_e = 1); the bead has then a normalized radius $R_b = r_b / r_e$. To simulate optical tweezers experiments, the bead is contacted to the substrate surface and centered at a normalized projected distance from the UME center, $L = d / r_e$. For levitating bead, as in Figure 2, approaching the center of the UME in the vertical direction, the bead is centered at an *altitude* $z_c = z + r_b$, where z is the projected bead-UME separation distance. In dimensionless form, the bead is centered at the altitude, $Z_c = z_c / r_e = Z + R_b$ with $Z = z / r_e$, the dimensionless bead-UME separation distance. The simulation consists of the numerical solution of the diffusion equation of the redox probe under the appropriate boundary conditions. The UME current, i_{el}, was evaluated from the concentration flux of the redox probe at the UME surface, where it is consumed, using the weak constraint procedure. The simulated curves relating the UME current, i_{el}, as a function of the projected bead center position (L, Z_c) have been generated by steady-state simulation. To better appreciate the impact of redox probe diffusion hindrance toward the UME by the bead, the UME current is expressed, as in SECM, in a dimensionless form, $I = i_{el} / i_{el,nb}$, where the current is normalized by the electrode current at the same electrode in the absence of the bead, $i_{el,nb}$ (I = 1 in the absence of the bead).

The contact of the bead with the substrate surface causes some meshing problems and undefined

inverted geometric regions. To optimize the meshing procedure and avoid the presence of undefined regions and minimize calculation errors, the contact of the bead with a plane was defined by a small bead-surface separation distance $Z = \varepsilon = 0.005$. We confirmed in the more accurate 2D-axisymmetric simulation that for $L = 0$ (bead and UME centered) the situation of pure bead-electrode contact was indistinguishable from that of a bead levitating at $\varepsilon = 0.005$, as the UME current variation between these two configurations was < 0.5%. The 2D-axisymmetric representation of the centered bead-electrode ($L = 0$) configuration was also used to optimize the meshing procedure in the 3D configuration so that the computation yielded the same UME current with < 1% difference under both 2D-axisymmetric and 3D simulation modes. For $L > 0$, the simulations are performed in 3D with the meshing procedure optimized for $L = 0$.

The electrode may be recessed relatively to the plane of the insulating sheath of normalized thickness $H = h / r_e$. The simulation then considers that the beads are either in contact with the insulating sheath for $L > 1$ and its center is at the altitude $Z = R_b + H + \varepsilon$ or in direct contact with the electrode for $L < 1$ and its center is at the altitude $Z = R_b + \varepsilon$. This situation also generates a region on the electrode that is forbidden by the bead.

RESULTS & DISCUSSION

The experimental set-up combines optical tweezers and a transparent UME. An ITO-coated glass cover slip is insulated by a thin silica layer which defines a disk-shaped UME of radius r_e (Figure 1). The thickness of the insulating silica layer defining the disk UME is 300 nm and therefore the microfabricated UMEs are slightly recessed and this was considered in the simulation procedures. The beads are here non-electroactive contrary to experiments reported by Aoki et al. with polyaniline-coated latex particles.[8]

Levitating beads above UME

A latex bead of radius r_b is picked up and trapped on the axis of a weakly focused laser beam through an objective lens. Argon ion and He-Ne lasers are used for levitation of the bead and for probing its position, respectively. The Argon ion laser acts as a 2-dimensional trap, and allows lifting up the particle. If the laser power is decreased, the particle gently moves down towards the UME at a controlled speed, under the action of its own weight (sedimentation) and of the radiation pressure. The distance z between the particle bottom and the UME is measured by means of an interference signal with the He-Ne laser, following the principle of RICM.[36] So both the position and the approach speed of the bead are optically controlled and determined.

In a configuration similar to the SECM, the UME mass-transfer limited current is measured while the bead is approached toward the UME center. The UME current is then expected to decrease when the bead approaches the UME as a result of the penetration of the bead in the diffusion field of the UME. The maximum current decrease is expected when the bead contacts the UME. Two examples of such approach curves are presented in Figure 2 when a bead with a 7.5 μm radius is approached to the center of UMEs of 15 and 25 μm radii, respectively. This was obtained by approaching the bead at known approach rates decreasing from v_b = 5 μm/s to 0.01 μm/s with decreased bead-UME vertical separation distances, z. During the bead approach, the evolution of the UME current with z is recorded. The experimental approach curves are then compared to the simulated ones (solid lines in Figure 2). The comparison is provided in dimensionless form, from the adjustment of the UME current (normalized by the current in the absence of bead). The agreement between experiments and simulations is rather good despite the small UME current variations. Owing to the small size of the bead compared to the UME dimension, the bead impact on the UME diffusion field is weak. The maximum decrease in the UME current detected experimentally is respectively 2.2% and 5.6% (with confidence higher than 0.5%) for the 25 and 15 μm radii UMEs, respectively. The current variation is small but the continuous current measurement by chronoamperometry ensures high confidence with small standard deviations. The

approach curves are performed within less than 8 s and the smallest 2.2% current decrease is too high to be assigned to long-term current drift. Clearly, the detected variations even though small are significantly evidencing the intrusion of the bead within the UME diffusion field. The accuracy is sufficient from such an approach to evaluate the indirect electrochemical localization of the bead in the vicinity of the UME, not only when the bead is in contact but also when it is levitating close to the UME. Note that even though the considered beads are smaller than the UME (r_b = 0.3 x r_e or 0.5 x r_e, respectively) they can be efficiently detected when they are levitating at distances lower than the UME radius ($z < r_e$).

The good agreement between experiments and simulation suggests that the contributions of convective mass-transfer from both the approach speed[38-40] and the possible local heating of the solution from the optical tweezers are negligible (see section 1 of Supporting information for a detailed discussion on both points). The contribution of convective mass transfer to the UME current is indeed small at low Péclet number ($Pe = v_b \ r_e / D$ with D the diffusion coefficient of the redox probe). We estimate $Pe < 0.1$ for most of the configurations investigated here (see Supporting information), indicating that the electrochemical signal is recorded in conditions of quasi-static regime.

Static beads

The optical tweezers setup uses an infrared laser, tightly focused through a high N.A. objective. The experiment starts by the optical trapping of a latex bead which is then positioned precisely on the surface of the glass slide at a center-to-center distance d of the UME (Figure 1B). To avoid local heating and uncontrolled convection, all further voltammetric experiments were recorded with the laser switched off.

The position of the bead is determined using the images acquired with the microscope. Figure 3A shows microscopy images of a bare UME (r_e = 6 μm). A bead of radius r_b = 7.5 μm was then optically trapped and positioned on the center of the same UME (Figure 3B). The dashed circle indicates the position of

the UME under the bead. Cyclic voltammograms for the reduction of $Ru(NH_3)_6^{3+}$ were recorded at a scan rate of 10 $mV.s^{-1}$. Figure 3E shows the experimental (solid lines) and the simulated (dashed lines) voltammograms. The bare UME displays a sigmoidal-shaped voltammogram which is characteristic of hemispherical diffusion (Figure 3C). The current intensity is in perfect agreement with the theoretical value for a slightly-recessed disk UME (Figure 3E). When the bead is positioned at the center of the UME (d = 0, Figure 3B), the shape of the voltammetric signal remains the same but the current is diminished from -7.7 nA to -5.6 nA. Indeed, as confirmed by computation of the $Ru(NH_3)_6^{3+}$ concentration profiles (Figure 3C-D), the presence of the bead in the vicinity of the UME partially blocks the depletion of the redox $Ru(NH_3)_6^{3+}$ species. The corresponding diffusional hindrance results in the decrease of the reduction current compared to the bare surface (Figure 3E) in good agreement with numerical simulation.

Incidentally, after the electrochemical measurements, the particle was removed from the UME using again the optical tweezers. Therefore one may tune the residence time of the bead on the UME. As expected, the current then raised back to its initial value (*i.e.* bare UME). One could argue that such a decrease of 27% is not so important if we consider the size of the electrode and of the blocking object. In fact, it illustrates a fundamental characteristic of the microelectrode for which hemispherical diffusion is predominant compared to linear one. As demonstrated in Figure 3D, even though the presence of the bead strongly perturbs the concentration field (see the isoconcentration > 85% which intersect the bead surface – blue line), at longer distance from the bead, the concentration profile remains hemispherical (see the 95% isoconcentration curve – dark blue line). Finally, the presence of the bead constrains the diffusion field of the UME to a smaller volume. Indeed, in the absence of the bead, the action of the UME (more than 5% consumption of the redox probe, the farthest isoconcentration line from the UME in Figure 3C – dark blue line) is located at a hemispherical surface of radius 10 times the UME radius. Meanwhile, in the presence of the bead, the same UME action is manifested in a smaller hemisphere of radius 7 times the UME radius (the farthest dark blue

isoconcentration line in Figure 3D). As proposed earlier,[1] the effect of the bead on the electrode current consists mainly in the decrease in the void volume within the diffusion field of the UME. This is confirmed in the simulated results of Figure S9 which addresses the effect of the radius of a bead centered on the UME on the current.

The above results also suggest that the extent of diffusion hindrance and the UME current will be sensitive to the localization of the bead on the UME (see Figure S9 for simulated current values and Figure S10 for simulated concentration profiles). Particularly, preferential disturbance of edge diffusion *vs.* diffusion to the center can be expected (see Figure S8 for simulated current values or Figure S10 for simulated concentration profiles). Indeed, as demonstrated in Figure S9B, when a bead smaller than the UME ($r_b < r_e$) is positioned close to the edge of the UME, it is predicted to have actually a higher blocking effect than when it is positioned at the UME center. For larger beads, such edge effect does not manifest anymore and the blocking effect of the bead increases continuously as the bead is approached toward the electrode center. The effect on the voltammetric signal of the projected center-to-center distance, d, between the sphere and the UME was then studied experimentally. The bead was first positioned at d = 16 μm (Figure S6A) and then moved progressively with the optical tweezers closer to the center of the UME at d = 7.5 μm (Figure S6B). Finally, it was brought at the UME center. At each position, cyclic voltammograms were recorded. Figure S6C shows the comparison of the electrochemical responses for the naked UME (blue line) and for increasing distance d = (i) 0, (ii) 7.5 and (iii) 16 μm. When the bead of radius 6 μm is located at d = 16 μm from the UME, the current is slightly decreased compared to the bead-free situation. As the parameter d decreases, the influence of the bead hindrance becomes more important on the diffusion layer and it is clearly visible on the electrochemical signal. Hence, as expected, the steady-state current decreases progressively in correlation with the diffusional shielding effect of the bead.

Figure S7 shows the influence of the bead size on the steady-state current for a constant projected center-to-center distance d = 3.4 μm. The reduction current decreases when the size of the beads

increases. Indeed, as already mentioned, the natural inference is that the mass transfer of $Ru(NH_3)_6^{3+}$ to the electrode surface is more blocked by the intrusion of a more voluminous object (higher decrease of the void diffusion volume) in the diffusion field of the UME. As discussed in Figure 3D, the simulated concentration profiles presented in Figure S10 show how the intrusion of a bead in the vicinity of the UME constrains its diffusion field to a smaller volume. Figure 4A shows a comparison of the normalized current for different bead-electrode distances and for different values of r_b and r_e. Using such plots, the position of a bead of given size can be extracted from the current intensity. It demonstrates that a bead can be detected electrochemically by an UME even when it does not hit the UME surface but when it enters its diffusion field and deforms it sufficiently to alter the UME current. If the maximal current decrease is observed for beads hitting directly the electroactive region of the UME ($d < r_e$), the precise localization of the bead on this region is difficult as the current value does not change significantly for $d < r_e$. Conversely, for $d > r_e$ even though lower current decrease is observed, the current is more sensitive to the bead-UME center-to-center distance allowing for a more precise localization of the bead. If one allows a detectable 3% variation of the UME current, beads of dimension comparable to the sensing UME can be detected when they are at distances $d < 0.7\ r_e + 1.4\ r_b$. Finally, Figure 4B nicely illustrates the good agreement between experimental data and the numerical modeling. It demonstrates that the efficient localization of beads in the vicinity of an UME can be achieved from their electrochemical signature.

Microbead assemblies

The electrochemical localization of a bead in the diffusion field of the UME is based on the occupancy of the diffusion field volume of the UME by the bead. Such a principle may then also be used to detect the successive arrival of other particles and their assembly in the vicinity of the UME. Optical tweezers allow one to manipulate particles with 50-nm precision. Therefore, we positioned successively single particles on the UME surface and recorded the corresponding steady-state currents.

When a first 3-µm radius bead is placed on the 6-µm radius UME surface (Figure 5B), the current decreases by 7 % from – 9.7 nA to – 9 nA (Figure 5E). Then, a second bead is optically deposited on the UME (Figure 5C) also blocking the mass transfer. In this case, the current decreases by 10.6 % from its initial value (i.e. bare UME). The experimental data are in excellent agreement with the numerical calculation. A third bead is approached with the optical tweezers but it has almost no effect on the current even though simulations predict an additional drop of 5 % for the current. This discrepancy is mainly related to the position of the bead. Indeed, a close inspection of Figure 5D shows that this third bead is slightly out of focus with a brighter ring around it. This implies that the particle was not located directly on the electrode surface but a few microns above. In fact, during its approach, the bead adhered to the other ones presumably by Van der Waals interactions and therefore its blocking effect was negligible due to its upper position. We finally approached a fourth bead further from the electrode (Figure 5D) and it did not affect the current, as expected for such a distance. In another kind of experiments, we trapped bead assemblies that were present in solution. Indeed, such aggregates easily form in solution containing supporting electrolytes because of electrostatic screening. Figure 6A displays the UME which was partially blocked by a 6-bead ensemble. As in previous experiments, the steady-state current is decreased due to diffusional hindrance of the beads (Figure 6B). These experiments show that single particles or more complex structures may be manipulated in a contactless mode near the UME surface.

CONCLUSION

We have shown that optical tweezers allow 3D manipulation of single levitating or static bead near UME. The steady-state current is thus modulated due to the diffusional hindrance of the non-conductive particle, allowing 3D localization of the bead in the vicinity of the UME. The residence time of the bead on the electrode surface is easily controlled by this contactless approach based on optical forces. Moreover, the electrode surface can be blocked by more complex structures such as ordered

arrangements of several beads and we studied their effects on the voltammetric signals. Since optical tweezers may trap living or smaller objects, this approach could be extended to electrochemical analysis of single nanoparticles and living cells, even if issues related to convection should not be underestimated.

ACKNOWLEDGEMENTS.

We thank L. Leroy, L. Couraud, D. Chouteau, X. Lafosse, J.-C. Esnault, and O. Mauguin for technical assistance during microfabrication in the LPN clean room. This work was supported by the Agence Nationale de la Recherche (Programme Blanc) and by the French Ministry of Foreign Affairs (PHC Procope).

REFERENCES

(1) Newton, M. R.; Morey, K. A.; Zhang, Y.; Snow, R. J.; Diwekar, M.; Shi, J.; White, H. S. *Nano Lett.* **2004**, *4*, 875.
(2) Zook, L. A.; Leddy, J. *J. Phys. Chem. B* **1998**, *102*, 10013.
(3) Monson, C. F.; Majda, M. *Anal. Chem.* **2007**, *79*, 9315.
(4) Newton, M. R.; Bohaty, A. K.; White, H. S.; Zharov, I. *J. Am. Chem. Soc.* **2005**, *127*, 7268.
(5) Cichelli, J.; Zharov, I. *J. Am. Chem. Soc.* **2006**, *128*, 8130.
(6) Chang, C.-Y.; Takahashi, Y.; Murata, T.; Shiku, H.; Chang, H.-C.; Matsue, T. *Lab Chip* **2009**, *9*, 1185.
(7) Chen, J.; Aoki, K.; Nishiumi, T.; Li, T. *Langmuir* **2006**, *22*, 10510.
(8) Aoki, K.; Lei, T. *Langmuir* **2000**, *16*, 10069.
(9) Ktari, N.; Quinson, J.; Teste, B.; Siaugue, J.-M.; Kanoufi, F.; Combellas, C. *Langmuir* **2012**, *28*, 12671.
(10) Nunes Kirchner, C.; Tra□uble, M.; Wittstock, G. *Anal. Chem.* **2010**, *82*, 2626.
(11) Scholz, F. *J. Solid State Electrochem.* **2011**, *15*, 1699.
(12) Davies, T. J.; Lowe, E. R.; Wilkins, S. J.; Compton, R. G. *ChemPhysChem* **2005**, *6*, 1340.
(13) Chang, Y.-L.; Palacios, R. E.; Fan, F.-R. F.; Bard, A. J.; Paul F. Barbara, P. F. *J. Am. Chem. Soc.* **2008**, *130*, 8906.
(14) Fan, F.-R. F.; Bard, A. J. *Nano Lett.* **2008**, *8*, 1746.
(15) Xiao, X.; Bard, A. J. *J. Am. Chem. Soc.* **2007**, *129*, 9610.
(16) Quinn, B. M.; van 't Ho, P. G.; Lemay, S. G. *J. Am. Chem. Soc.* **2004**, *126*, 8360.
(17) Alligrant, T. M.; Nettleton, E. G.; Crooks, R. M. *Lab on a Chip* **2013**, *13*, 349.
(18) Zhou, Y.-G.; Rees, N. V.; Pillay, J.; Tshikhudo, R.; Vilakazi, S.; Compton, R. G. *Chem. Commun.* **2012**, *48*, 224.

(19) Kleijn, S. E. F.; Lai, S. C. S.; Miller, T. S.; Yanson, A. I.; Koper, M. T. M.; Unwin, P. R. *J. Am. Chem. Soc.* **2012**, *134*, 18558.
(20) Boika, A.; Thorgaard, S. N.; Bard, A. J. *J. Phys. Chem. B* **2012**, *117*, 4371.
(21) Fosdick, S. E.; Anderson, M. J.; Nettleton, E. G.; Crooks, R. M. *J. Am. Chem. Soc.* **2013**, *135*, 5994.
(22) Davies, T. J.; Banks, C. E.; Compton, R. G. *J. Solid State Electrochem.* **2006**, *9*, 797–808.
(23) Fietkau, N.; Chevallier, F. G.; Jiang, L.; Jones, T. G. J.; Compton, R. G. *ChemPhysChem* **2006**, *7*, 2162.
(24) Fietkau, N.; Du, G.; Matthews, S. M.; Johns, M. L.; Fisher, A. C.; Compton, R. G. *J. Phys. Chem. C* **2007**, *111*, 13905.
(25) Rees, N. V.; Matthews, S. M.; Yunus, K.; Fisher, A. C.; Compton, R. G. *Angew. Chem. Int. Ed.* **2009**, *48*, 2376.
(26) Lee, S.; Zhang, Y.; White, H. S.; Harrell, C. C.; Martin, C. R. *Anal. Chem.* **2004**, *76*, 6108.
(27) Zhang, B.; Zhang, Y.; White, H. S. *Anal. Chem.* **2006**, *78*, 477.
(28) Gosse, C.; Croquette, V. *Biophys. J.* **2002**, *82*, 3314.
(29) Jonáš, A.; Zemánek, P. *Electrophoresis* **2008**, *29*, 4813.
(30) Neuman, K. C.; Block, S. M. *Rev. Sci. Instrum.* **2004**, *75*, 2787.
(31) Ashkin, A.; Dziedzic, J. M.; Bjorkholm, J. E.; Chu, S. *Opt. Lett.* **1986**, *11*, 288.
(32) Zemánek, P.; Jonás, A.; Srámek, L.; Liska, M. *Opt. Lett.* **1999**, *24*, 1448.
(33) Liu, H.; Newton, G.; Nakamura, R.; Hashimoto, K.; Nakanishi, S. *Angew. Chem. Int. Ed.* **2010**, *49*, 6596.
(34) Ashkin, A.; Dziedzic, J. M. *Appl. Phys. Lett.* **1971**, *19*, 283.
(35) Ashkin, A. *Phys. Rev. Lett.* **1970**, *24*, 156.
(36) Raedler, J.; Sackmann, E. *Langmuir* **1992**, *8*, 848.
(37) Kraikivski, P.; Pouligny, B.; Dimova, R. *Rev. Sci. Instrum.* **2006**, *77*, 113703.
(38) Nkuku, C. A.; LeSuer, R. J. *J. Phys. Chem. B* **2007**, *111*, 13271.
(39) Cornut, R.; Poirier, S.; Mauzeroll, J. *Anal. Chem.* **2012**, *84*, 3531.
(40) Combellas, C.; Fermigier, M.; Fuchs, A.; Kanoufi, F. *Anal. Chem.* **2005**, *77*, 7966.

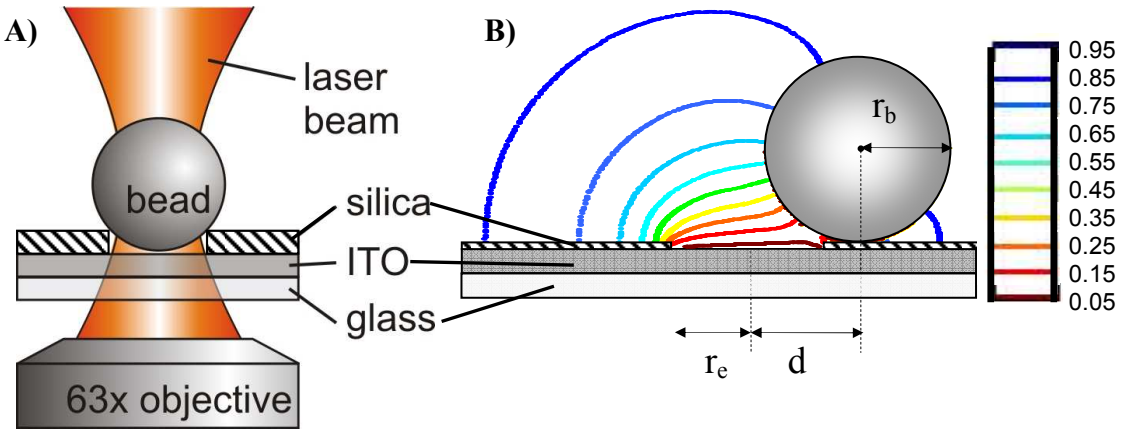

Figure 1. A) Experimental set-up showing the ITO UME and the latex bead trapped with a focused laser beam. The sketch is not to scale. B) Schematic (side-view) representation of the bead of radius r_b positioned at a projected center-to-center distance d of the disk UME of radius r_e. The bead is positioned on the insulating silica layer. The lines correspond to isoconcentration profiles in the vertical symmetry plane passing through the center of the bead and the center of the UME. At infinite distance from the electrode (bulk), the redox probe concentration is $C_0 = 1$ and it is consumed at the electrode ($C_e = 0$). The presented profiles are obtained for $r_e = 6$ µm, $r_b = 7.5$ µm and $d = 9$ µm.

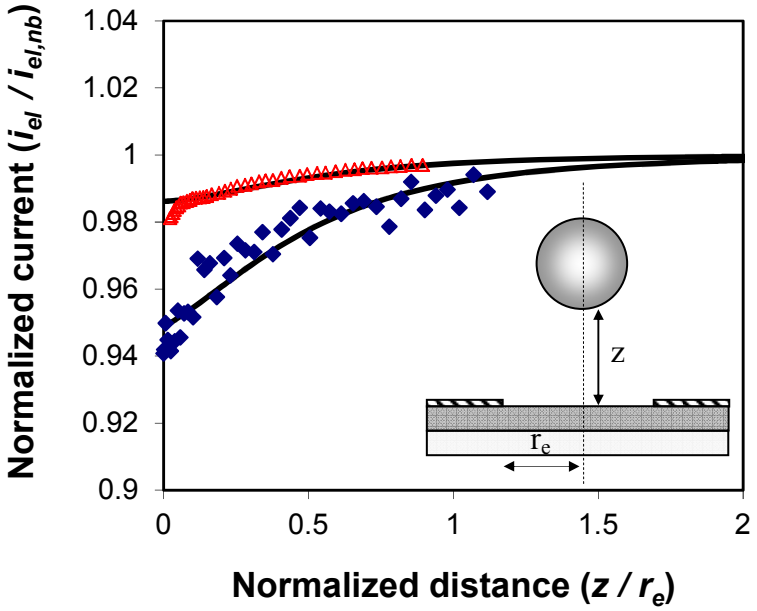

Figure 2. Approach curves of a levitating bead (r_b = 7.5 µm) to the center of a (◆) 15 or a (Δ) 25 µm radius UME (d = 0). Comparison of experimental (symbols) and simulated (solid lines) values of the UME current (i_{el}) normalized by the current in the absence of bead ($i_{el,nb}$) as a function of the projected bead-UME separation distance, z, normalized by the UME radius, r_e. UME currents were recorded in a solution containing 5 x 10^{-3} M $Ru(NH_3)_6^{3+}$ and 0.1 M Na_2SO_4 as supporting electrolyte.

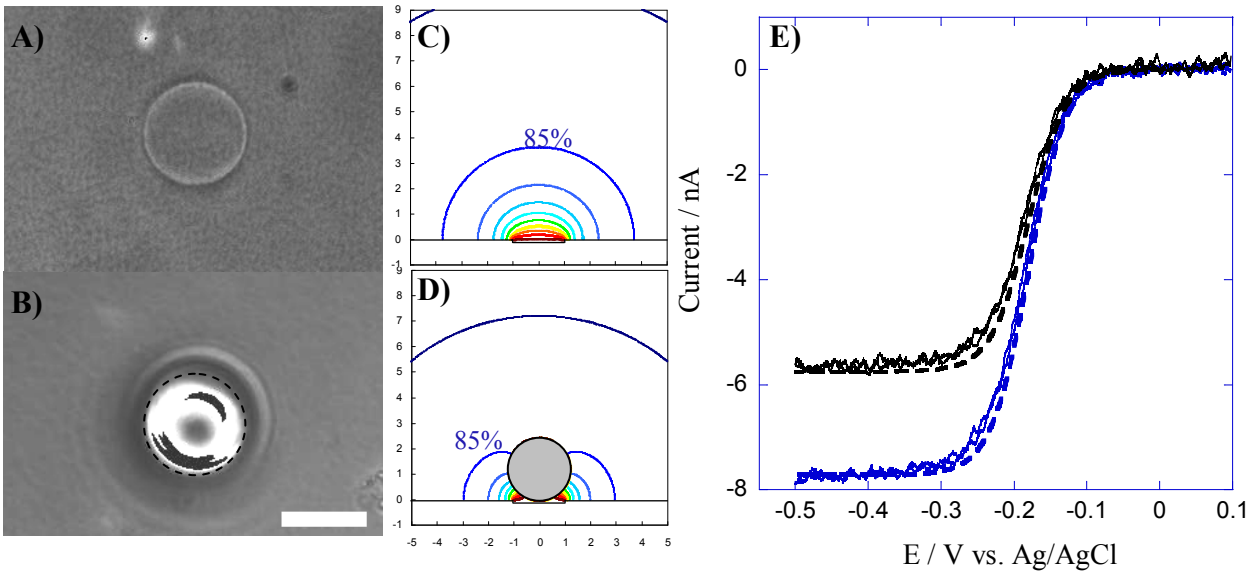

Figure 3. A,B) Top-view images of an UME of radius r_e = 6 µm without (A) or with (B) a bead of radius r_b = 7.5 µm which has been optically deposited on its center (d = 0). The dashed circle indicates the position of the electrode under the bead. Scale bar: 10 µm. Side-views of the simulated concentration profiles passing by the center of the UME (C) in the absence and (D) in the presence of the bead. The lines correspond to isoconcentration profiles with the same color scale as in Figure 1. E) Corresponding cyclic voltammograms for the electrode without (blue line) or with (black line) the bead positioned over its center. Cyclic voltammograms were recorded at a scan rate of 10 $mV.s^{-1}$ in a solution containing 5 x 10^{-3} M $Ru(NH_3)_6^{3+}$ and 0.1 M Na_2SO_4 as supporting electrolyte. Dashed lines represent simulated voltammograms.

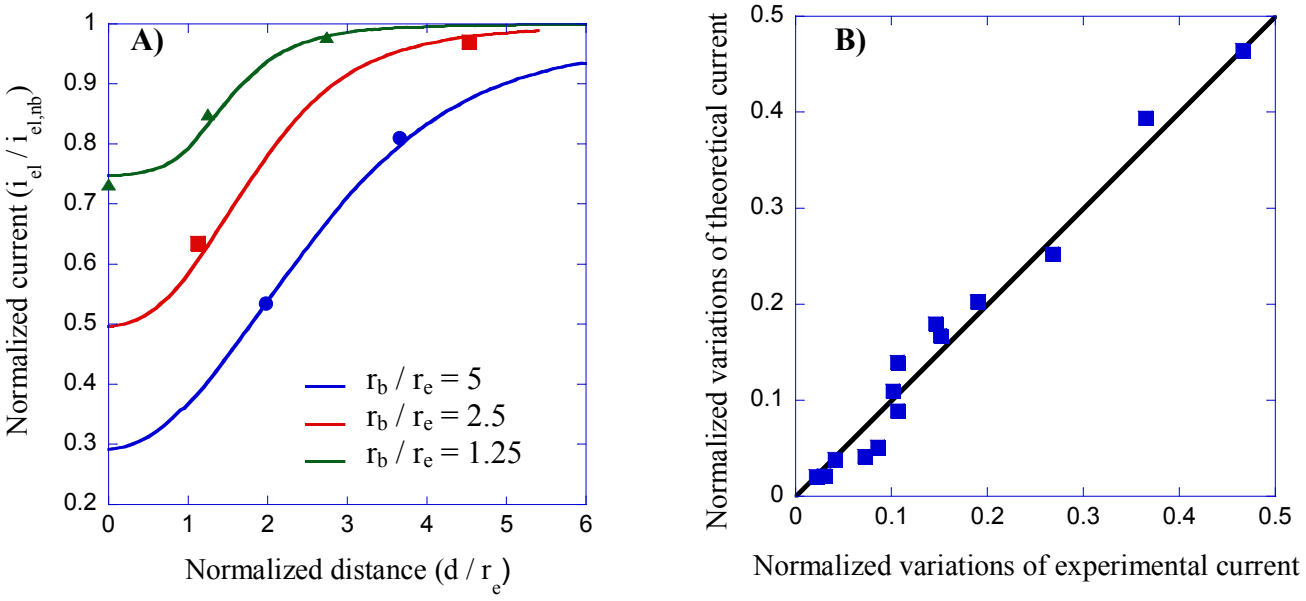

Figure 4. A) Comparison between the experimental points and the theoretical curves (solid lines) for the variations of the normalized stationary current for beads of radius r_b = 7.5 µm on UME of various radii r_e as a function of the projected normalized center-to-center distance d / r_e. Plotted experimental points correspond to r_e = 1.5 µm (r_b / r_e = 5, blue disks), r_e = 3 µm (r_b / r_e = 2.5, red squares) and r_e = 6 µm (r_b / r_e = 1.25, green triangles). B) Correlation between experimental (blue squares) and theoretical (solid line) current variations for various values of the parameters r_b, r_e and d.

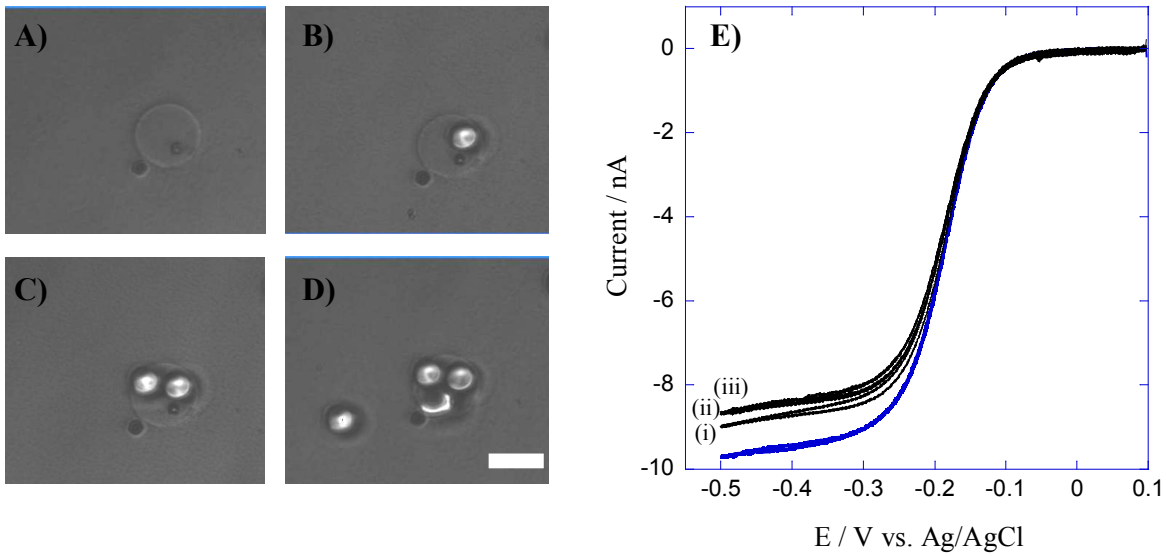

Figure 5. A-D) Images of an UME of radius r_e = 6 µm on which (A) 0, (B) 1, (C) 2 or (D) 3 beads of radius r_b = 3 µm were deposited using the optical tweezers. E) Corresponding cyclic voltammograms for the electrode without (blue line) or with (i) 1, (ii) 2 or (iii) 3 beads positioned on its surface. Same experimental conditions as in Figure 2. Scale bar: 10 µm.

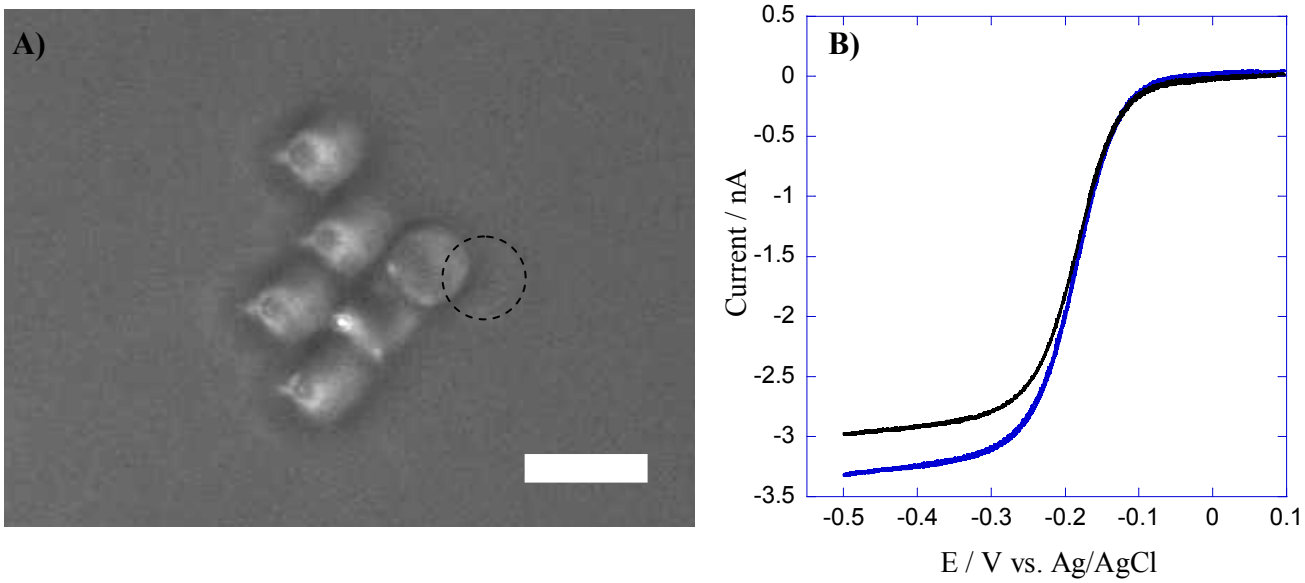

Figure 6. A) Image of an UME of radius r_e = 3 µm partially covered with 6 beads of radius r_b = 3 µm which were deposited using the optical tweezers. B) Corresponding cyclic voltammograms for the electrode without (blue line) or with the 6 beads (black line). The center-to-center distance between the electrode and the closest bead is 4.8 µm. Same experimental conditions as in Figure 2. The dashed circle materializes the position of the electrode under the bead. Scale bar: 10 µm.

Figure for TOC